I&EC research
Industrial & Engineering Chemistry Research

Article

pubs.acs.org/IECR

Carotenoid Production Process Using Green Microalgae of the *Dunaliella* Genus: Model-Based Analysis of Interspecies Variability

Melanie Fachet,[†] Robert J. Flassig,[†] Liisa K. Rihko-Struckmann,[*,†] and Kai Sundmacher[†,‡]

[†]Process Systems Engineering, Max Planck Institute for Dynamics of Complex Technical Systems, Magdeburg, 39106, Germany
[‡]Process Systems Engineering, Otto von Guericke University Magdeburg, Magdeburg, 39106, Germany

Supporting Information

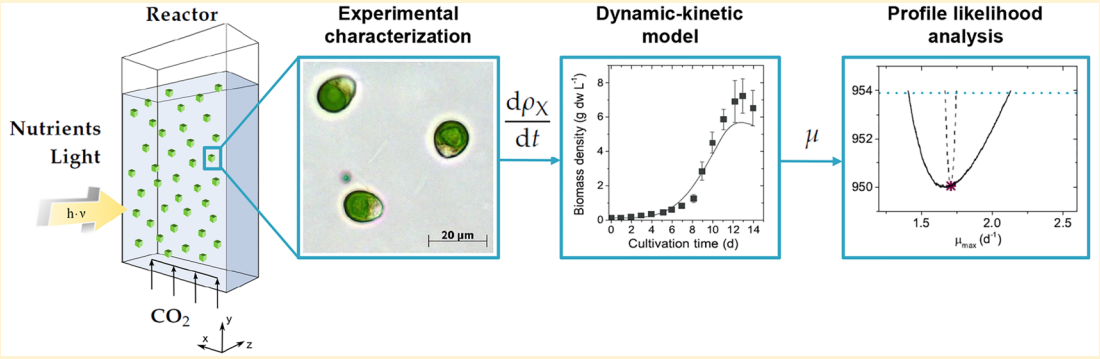

ABSTRACT: The engineering of photosynthetic bioprocesses is associated with many hurdles due to limited mechanistic knowledge and inherent biological variability. Because of their ability to accumulate high amounts of β-carotene, green microalgae of the *Dunaliella* genus are of high commercial relevance for the production of food, feed, and high-value fine chemicals. This work aims at investigating the interspecies differences between two industrially relevant *Dunaliella* species, namely *D. salina* and *D. parva*. A systematic work flow composed of experiments and mathematical modeling was developed and applied to both species. The approach combining flow cytometry and pulse amplitude modulation (PAM) fluorometry with biochemical methods enabled a coherent view on the metabolism during the adaptational stress response of *Dunaliella* under carotenogenic conditions. The experimental data was used to formulate a dynamic-kinetic reactor model that covered the effects of light and nutrient availability on biomass growth, internal nutrient status, and pigment fraction in the biomass. Profile likelihood analysis was performed to ensure the identifiability of the model parameters and to point out targets for model reduction. The experimental and computational results revealed significant variability between *D. salina* and *D. parva* in terms of morphology, biomass, and β-carotene productivity as well as differences in photoacclimation and photoinhibition. The synergistic approach combining experimental and mathematical methods provides a systems-level understanding of the microalgal carotenogenesis under fluctuating environmental conditions and thereby drive the development of sustainable and economically feasible phototrophic processes.

INTRODUCTION

Halotolerant green microalgae of the *Dunaliella* genus are among the most important production organisms for natural β-carotene. The accumulation of the pigment is an adaption of the exposure to extreme environmental conditions such as high light intensity, high salinity, and nutrient starvation. The overaccumulation of carotenoid pigments is due to a stress response which enables *Dunaliella* to survive in hypersaline environments. *Dunaliella* sp. occur in saline shallow lakes and evaporation ponds all over the world.[1] Beside hypersaline species in the genus *Dunaliella* several euryhaline species of *Dunaliella* (e.g., *D. tertiolecta* and *D. primolecta* have been reported, which grow in marine water. However, only the hypersaline species of the *Dunaliella* genus (e.g., *D. parva*, *D. viridis*, and *D. salina*) play an important role in algal mass cultivation.[2]

There have been very few studies dealing with a comparative evaluation of physiological and biochemical differences among microalgal strains or species. However, when they exist they generally indicate a significant intra- and interspecies variability which makes comparison of results and deduction of valuable conclusions challenging among different strains.[3] Because of its high β-carotene content, the majority of the studies focused on the biotechnological potential of *D. salina*. This work aims at investigating the interspecies differences between two carotenogenic *Dunaliella* strains, namely *D. salina* and *D. parva*. A

Special Issue: Tapio Salmi Festschrift

Received: April 20, 2017
Revised: June 26, 2017
Accepted: July 5, 2017
Published: July 5, 2017

DOI: 10.1021/acs.iecr.7b01423
Ind. Eng. Chem. Res. XXXX, XXX, XXX−XXX

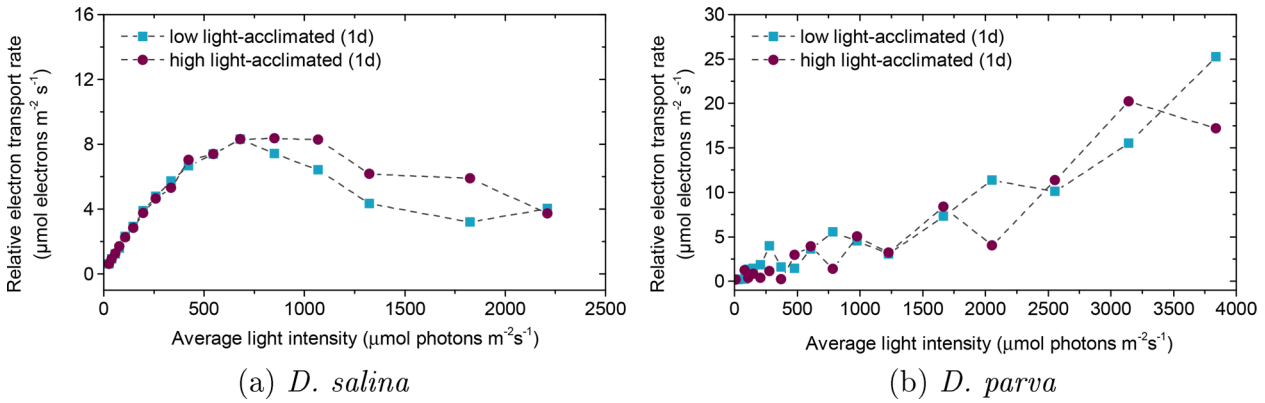

Figure 1. Relationship between electron transport rate and average light intensity in *D. salina* (a) and *D. parva* (b).

special emphasis was placed on the morphological differences, the productivity in terms of biomass and β-carotene, and the adaptational stress response as well as differences in photoacclimation and photoinhibition. For this purpose, an interdisciplinary work flow composed of experiments and mathematical modeling was developed and applied to *D. salina* and *D. parva*.

MATERIALS AND METHODS

Strain, Growth Medium, and Precultivation. The strains *D. salina* and *D. parva* used in this work were obtained from the Culture Collection of Algae and Protozoa (Windermere, United Kingdom) and identified based on 18S rRNA sequencing. The growth of both stock cultures was performed in a rotary shaking incubator (Multitron, Infors AG, Switzerland) in 3.5% CO_2 enriched air, at a temperature of 26 °C, with 100 rpm rotational speed and a light intensity of 30 μmol photons m^{-2} s^{-1} applied in alternating day/night cycles (16 h/8 h). The growth medium composition was as follows: 1.50 M NaCl, 22.50 mM Na_2SO_4, 4.87 mM K_2SO_4, 1.00 mM NaH_2PO_4, 0.37 mM $MgCl_2$, 19.35 mM Na_2EDTA, 18.9 mM $CaCl_2$, 11.25 mM NaFe EDTA, 1.89 mM $MnCl_2$, 1.48 mM $ZnSO_4$, 0.67 mM $CuSO_4$, 10.95 nM Na_2MoO_4, and 9.95 nM $CoCl_2$. The nitrogen-replete medium contained 37.75 mM KNO_3, whereas the nitrogen-depleted medium contained an equimolar content of KCl.

Cultivation Experiments in Flat-Plate Photobioreactors. Cultivations were performed in flat-plate photobioreactors either with 1 L cultivation volume (FMT 150, Photon Systems Instruments) equipped with white and red LEDs (for *D. parva*) or with 1.8 L cultivation volume (Labfors Lux, Infors HT) equipped with warm white LEDs (for *D. salina*). Both reactors were bubbled with a gas mixture of 97% air and 3% CO_2 at 500 mL min^{-1} flow rate provided by mass flow controllers. The pH was maintained at 7.5 by the addition of 1 M HCl and 1 M KOH, and the temperature was set to 24 °C. An optical pO_2 electrode (Visiferm DO, Hamilton Messtechnik GmbH, Switzerland) was used to measure the dissolved oxygen concentration in the reactors. The transmitted light intensity was determined using a light sensor on the backside of the reactor (ULM-500, Walz or Infors HT).

Carbon and Nitrogen Fraction in the Biomass. The carbon and nitrogen cell quota of the biomass were determined by C/H/N analysis from freeze-dried samples (Currenta, Germany).

Ion Chromatography. Extracellular nitrogen density was measured by ion chromatography (Dionex ICS 1100, Thermo Scientific Dionex, USA) using an Ion Pak AS22 column (Thermo Scientific Dionex, USA) with 4.5 mM sodium carbonate and 1.4 mM sodium bicarbonate as mobile phase at a flow rate of 1.2 mL min^{-1} and with an injection volume of 50 μL.

Spectrophotometrical Determination of Chlorophyll and Carotenoid Fractions. UV/vis spectrophotometry was used to measure the carotenoid and chlorophyll fractions in the biomass. Briefly, a 3−10 mL sample was taken from the reactor depending on the cell density and pigment fraction. After the cells were filtered onto glass microfiber filters (GF/F, 0.7 μm, Whatman, UK), a washing step with 0.5 M ammonium formate, followed by the addition of 6 mL of 90% acetone was performed. The pigment extract was incubated for 1 h at 4 °C in a mixing block at 100 rpm. The mixture was centrifuged 5 min at 3000*g* to separate the cell debris from the pigment extract. The supernatant was measured with a spectrophotometer (Specord S600, Analytik Jena, Germany) at 470, 645, and 661.5 nm. The pigment densities of the sample were calculated according the equations given below.[4]

$$c_{\mathrm{Chla}} = (11.24A_{661} - 2.04A_{645})$$

$$c_{\mathrm{Chlb}} = (20.13A_{645} - 4.19A_{661})$$

$$c_{\mathrm{Car}} = \frac{(1000A_{470} - 1.9c_{\mathrm{Chla}} - 63.14c_{\mathrm{Chlb}})}{214}$$

Flow Cytometric Analysis. A flow cytometric measurement was conducted to determine the cell density in the reactor using volumetric counting of 200 μL culture suspension. Therefore, all samples were diluted to a cell density of approximately 1×10^6 cells mL^{-1} prior to analysis. Light scattering and fluorescence emission was excited with a blue argon solid state (488 nm) laser in a flow cytometer (CyFlow Space, Sysmex-Partec, Germany). The samples were measured with a flow rate of 1 μL s^{-1} in 1.5 M NaCl as sheath fluid.

Pulse Amplitude Modulation (PAM) Fluorometry. The relative electron transport rate (ETR) was measured using the Dual-PAM 100 fluorometer (Walz, Germany) as previously described in Fachet et al.[5] Briefly, 1.5 mL of cell sample was dark adapted for 10 min at 26 °C. Afterward, the minimal fluorescence level (F_0) and maximal fluorescence level (F_m) induced by a saturating actinic light pulse (635 nm, 2000 μmol photons m^{-2} s^{-1}, 0.5 s) were determined with a measuring radiation of 5 μmol m^{-2} s^{-1}. Subsequently, the actinic light was

DOI: 10.1021/acs.iecr.7b01423
Ind. Eng. Chem. Res. XXXX, XXX, XXX−XXX

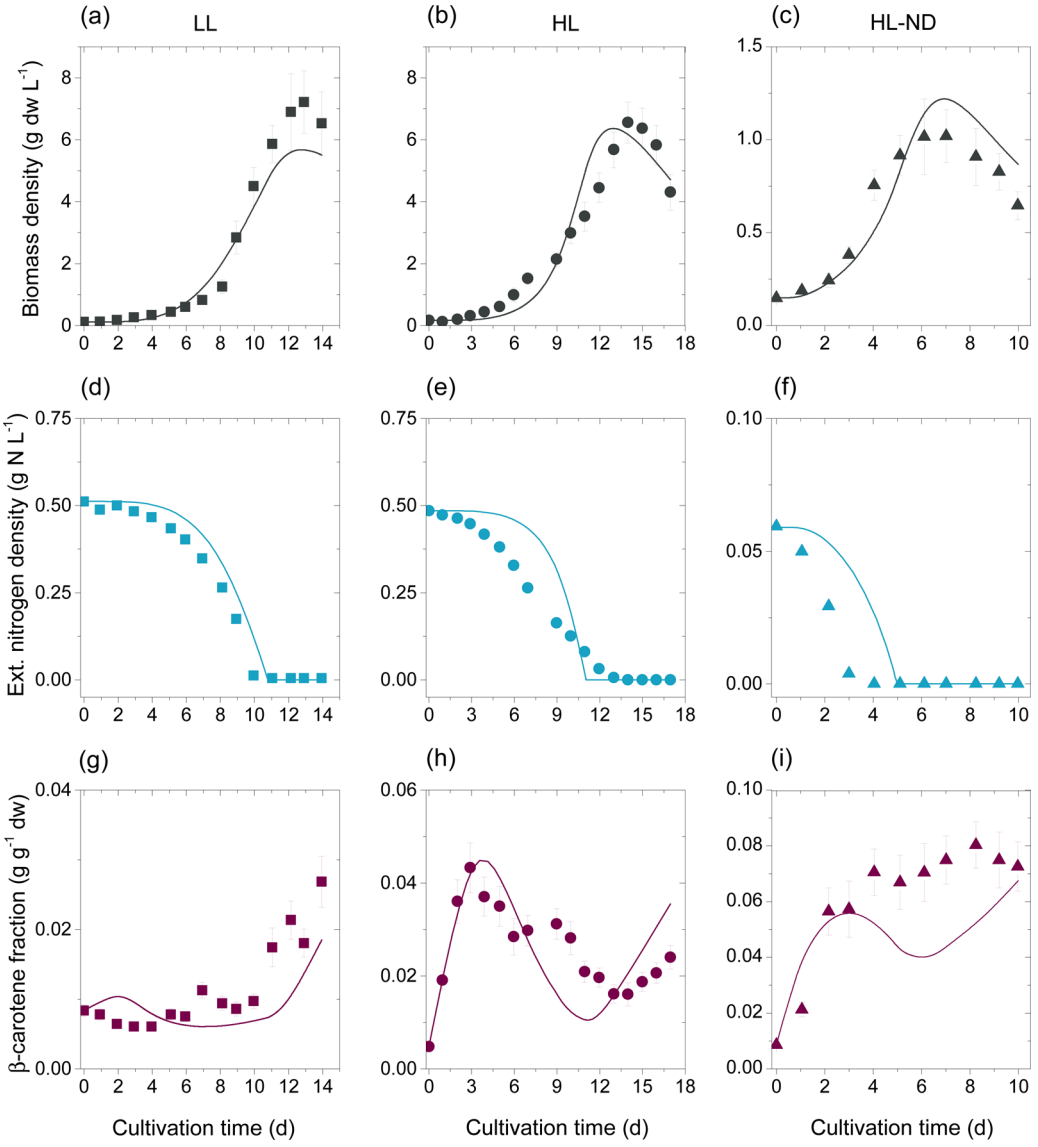

Figure 2. Model simulations for *D. salina* for the effect of various cultivation conditions on the biomass density $\rho_{X,dw}$ (a–c), the extracellular nitrogen density $\rho_{N,ext}$ (d–f) and the β-carotene fraction ω_{Car} (g–i). Comparison of the simulated time course (lines) with experimental data (symbols). The symbols represent the mean values and the error bars correspond to the standard deviation. An initial biomass density of 0.1 g dw L^{-1} was used for inoculation. The illumination of the reactor was performed as stated in Table S3 in the Supporting Information.

turned on to determine the photosynthetic parameters of the light adapted state. After the light-adapted fluorescence signal F' reached steady-state, a saturation pulse was applied to the culture which induced the closure of all reaction centers and the value for light-adapted maximal fluorescence F'_m was achieved.

RESULTS AND DISCUSSION

Strain Identification of *D. salina* and *D. parva*. Both strains were ordered from the Culture Collection of Algae and Protozoa (CCAP) and assigned based on morphological properties and 18S rRNA sequencing to *D. salina* (CCAP 19/18) and *D. parva* (CCAP 19/10). Both strains had a 100% query coverage (99% Max. ID) with *D. parva* and *D. salina*, respectively.

Experimental Analysis of Interspecies Variability. *Morphological Variability between D. salina and D. parva.* Beside *D. salina*, *D. parva* and *D. pseudosalina* are known to belong to the carotenogenic species of the *Dunaliella* genus.[6] Like *D. salina*, *D. parva* is a hypersaline alga tolerating NaCl fractions from 3% (w/w) NaCl to saturation and an optimal salinity range from 6 to 8% (w/w).[6] In contrast to *D. salina* which has a carotenoid content of 8 to 10% (w/w), the maximum carotenoid fraction reported for *D. parva* is about 5% (w/w).[6]

The most distinctive features between *D. salina* and *D. parva* were the cell size and the dry weight. The results of the comparison are shown in Supporting Information Table S1 and showed a high morphological and physiological variability among the studied species. The length of a single *D. parva* cell was only half the cell length of *D. salina* (7.6 μm compared to 14.6 μm) and the cell width was only one-third of *D. salina* (3.8 μm compared to 11.6 μm). The significant differences in the cell size also translated into the cellular dry weight. An average *D. parva* cell had a weight of only 33.5 pg $cell^{-1}$, whereas the *D. salina* cell had a weight of 520 pg $cell^{-1}$ when cultivated under low-light and nutrient-repleted conditions. The size measure-

DOI: 10.1021/acs.iecr.7b01423
Ind. Eng. Chem. Res. XXXX, XXX, XXX–XXX

Table 1. Optimal Parameter Values $\hat{\Theta}$ as Well as the Individual Confidence Intervals $[\sigma_i^-; \sigma_i^+]$ Corresponding to a Confidence Level of 95% from Constrained Nonlinear Optimization and Profile Likelihood Analysis for *D. salina*

strain	symbol	$\hat{\Theta}$	σ_i^-	σ_i^+	identifiability
D. salina	$r_{N,max}$	0.346	0.249	0.531	structurally and practically identifiable
	$K_{s,N}$	0.005	0.0003	3.591	structurally and practically identifiable
	μ_{max}	1.708	1.406	2.130	structurally and practically identifiable
	$K_{s,E}$	0.033	0.018	0.055	structurally and practically identifiable
	$K_{i,E}$	68.719	48.186	97.744	structurally and practically identifiable
	$E_{car,crit}$	77.718	74.102	80.138	structurally and practically identifiable
	$r_{car,E}$	0.032	0.022	0.041	structurally and practically identifiable
	$r_{car,N}$	0.005	0.0045	0.0055	structurally and practically identifiable
	r_R	0.142	0.131	0.152	structurally and practically identifiable

ments were in line with the values published by Borowitzka and Siva[6] and are given in Table S1 for comparison.

Biotechnological Parameters for Growth and β-Carotene Accumulation. Batch cultivations of *D. salina* and *D. parva* were carried out in order to identify interspecies differences in biomass formation and pigment accumulation (see Tables S2 and S3 for experimental conditions). The biotechnological parameters listed in Tables S4 and S5 indicated that *D. salina* outperformed *D. parva* in almost all cases. The highest content of β-carotene was observed under HL-ND conditions with 8.0% (w/w) for *D. salina* and 4.9% (w/w) for *D. parva* and is in line with values reported by Borowitzka and Siva.[6] Although the initial nitrate density of the HL-ND batch of *D. parva* was lower compared to the HL-ND batch of *D. salina* (0.017 g N L^{-1} compared to 0.05 g N L^{-1}), the incorporation into the biomass seems to be more efficient since the final biomass density for *D. parva* was 35% higher. Indeed, the elemental composition analysis revealed a minimum nitrogen cell quota of 0.02 g N g^{-1} dw for *D. parva* whereas 0.03 g N g^{-1} dw was measured for *D. salina* (Tables S6 and S7).

Photosynthetic Performance. The relative ETR is an indicator for the photosynthetic capacity of cells and therefore linked to the ability for providing energy for cell growth and metabolism. It is calculated as described in eq 1 by multiplication of the average light intensity ($\bar{E}$) with the effective quantum yield ($\Phi_{PSII,eff}$) and the default ETR factor of 0.42.[7] The default ETR factor originates from a "model" leaf and describes the fraction of the incident light intensity in the PAR region that is absorbed in PSII.

$$\mathrm{ETR} = 0.42\Phi_{\mathrm{PSII,eff}}\bar{E} = 0.42\frac{F'_m - F'}{F'_m}\bar{E} \quad (1)$$

The relationship between relative ETR and average light intensity for *D. salina* is shown in Figure 1a. The curve clearly shows the three characteristic phases (light limitation, light saturation, and photoinhibition). Under both conditions (low- and high-light acclimated cells), the ETR for *D. salina* increased linearly until a light intensity of 550 μmol photons m^{-2} s^{-1} was reached. In this light regime, the light intensity directly correlates with the rate of photosynthesis. Both cultures of *D. salina* reached a maximal ETR value of 6.9 to 8.3 μmol electrons m^{-2} s^{-1} (Figure 1a). The light saturation range for the low light-acclimated culture was from 550−860 μmol photons

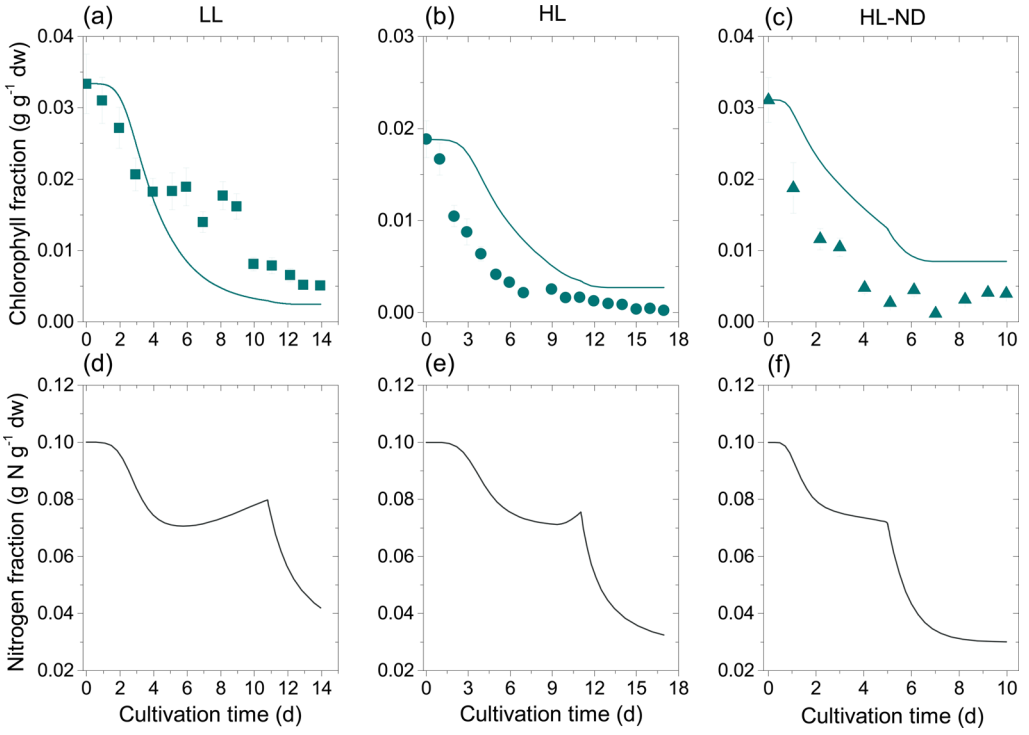

Figure 3. Model simulations for *D. salina* for the effect of various cultivation conditions on the chlorophyll fraction ω_{Chl} (a−c) and the nitrogen quota in the biomass ω_N (d−f). Comparison of the simulated time course (lines) with experimental data (symbols). The symbols represent the mean values and the error bars correspond to the standard deviation.

DOI: 10.1021/acs.iecr.7b01423
Ind. Eng. Chem. Res. XXXX, XXX, XXX−XXX

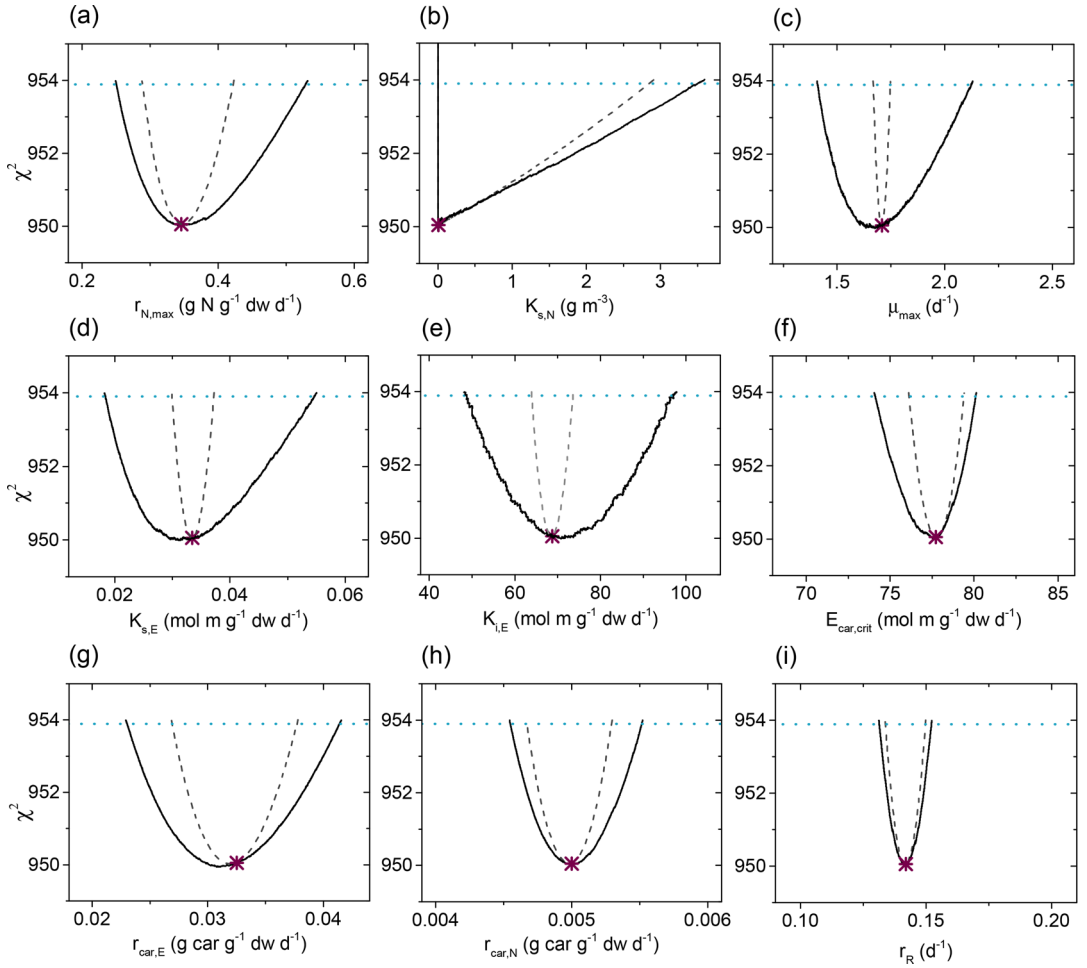

Figure 4. Profile likelihood-based identifiability for all model parameters for *D. salina*: (a) maximal nitrogen uptake rate r_{max}, (b) half-saturation coefficient for nitrogen uptake $K_{s,N}$, (c) maximal growth rate μ_{max}, (d) half-saturation coefficient for photosynthetic growth $K_{s,E}$, (e) light inhibition coefficient for photosynthetic growth $K_{i,E}$, (f) critical light intensity for β-carotene synthesis $E_{car,crit}$, (g) light stress-induced β-carotene synthesis rate $r_{car,E}$, (h) nutrient stress-induced β-carotene synthesis rate $r_{car,N}$ and (i) respiration rate r_R. The profile likelihood-based sensitivity curve, where Θ_i is varied and all other parameters $\Theta_{j\neq i}$ are kept constant, is indicated by the dashed gray line. The profile likelihood-based identifiability curves are indicated by the black solid line. The blue dotted horizontal line indicates the threshold utilized to assess likelihood-based 95% confidence interval and the asterisk corresponds to the optimal parameter value.

m^{-2} s^{-1}, whereas the high light-acclimated culture showed a prolonged light saturation phase from 550−1070 μmol photons m^{-2} s^{-1}. The light saturation phase is followed by a photoinhibition phase in which the ETR declined to about 4 μmol electrons m^{-2} s^{-1} at 2200 μmol photons m^{-2} s^{-1}.

Beside the differences in morphology and biotechnological parameters, further variability of *D. parva* compared to *D. salina* was observed in the response upon exposure to oversaturating light conditions as illustrated in Figure 1b, where the dependency of the ETR on the average light intensity is given. In contrast to *D. salina*, a pronounced saturation and photoinhibitory phase could not be observed, neither for low light nor for high light-acclimated *D. parva* cells. Because of the absence of a photoinhibition phase in *D. parva*, the maximal ETR of 25 μmol electrons m^{-2} s^{-1} is three times higher compared to the maximal ETR achieved for *D. salina*.

Dynamic-Kinetic Growth Model for *D. salina* and *D. parva*. In the following section, the interspecies variability between *D. salina* and *D. parva* was analyzed with a model-based approach, namely a dynamic-kinetic growth model. The experimental data for the simulations were obtained as specified in Tables S2 and S3.

Model Formulation. The presented dynamic−kinetic growth model is based on an ordinary differential equation (ODE) system published by Fachet et al.[8] with the extension to account for photoacclimation, photoinhibition, and β-carotene accumulation (see eqs 2 and 3). The following five state variables were considered:

- biomass density ρ_X (g dw m^{-3})
- extracellular nitrogen density ρ_N (g N m^{-3})
- intracellular nitrogen fraction ω_N (g N g^{-1} dw)
- chlorophyll fraction ω_{Chl} (g Chl g^{-1} dw)
- β-carotene fraction ω_{Car} (g Car g^{-1} dw)

The complete algebraic equation system can be found in the Supporting Information.

β-Carotene Synthesis Rate. The synthesis of β-carotene mainly depends on the presence and intensity of light and nutrient stress. Therefore, the equation for its synthesis couples a light-dependent and nutrient-dependent synthesis term as formulated below (eq 2):

DOI: 10.1021/acs.iecr.7b01423
Ind. Eng. Chem. Res. XXXX, XXX, XXX−XXX

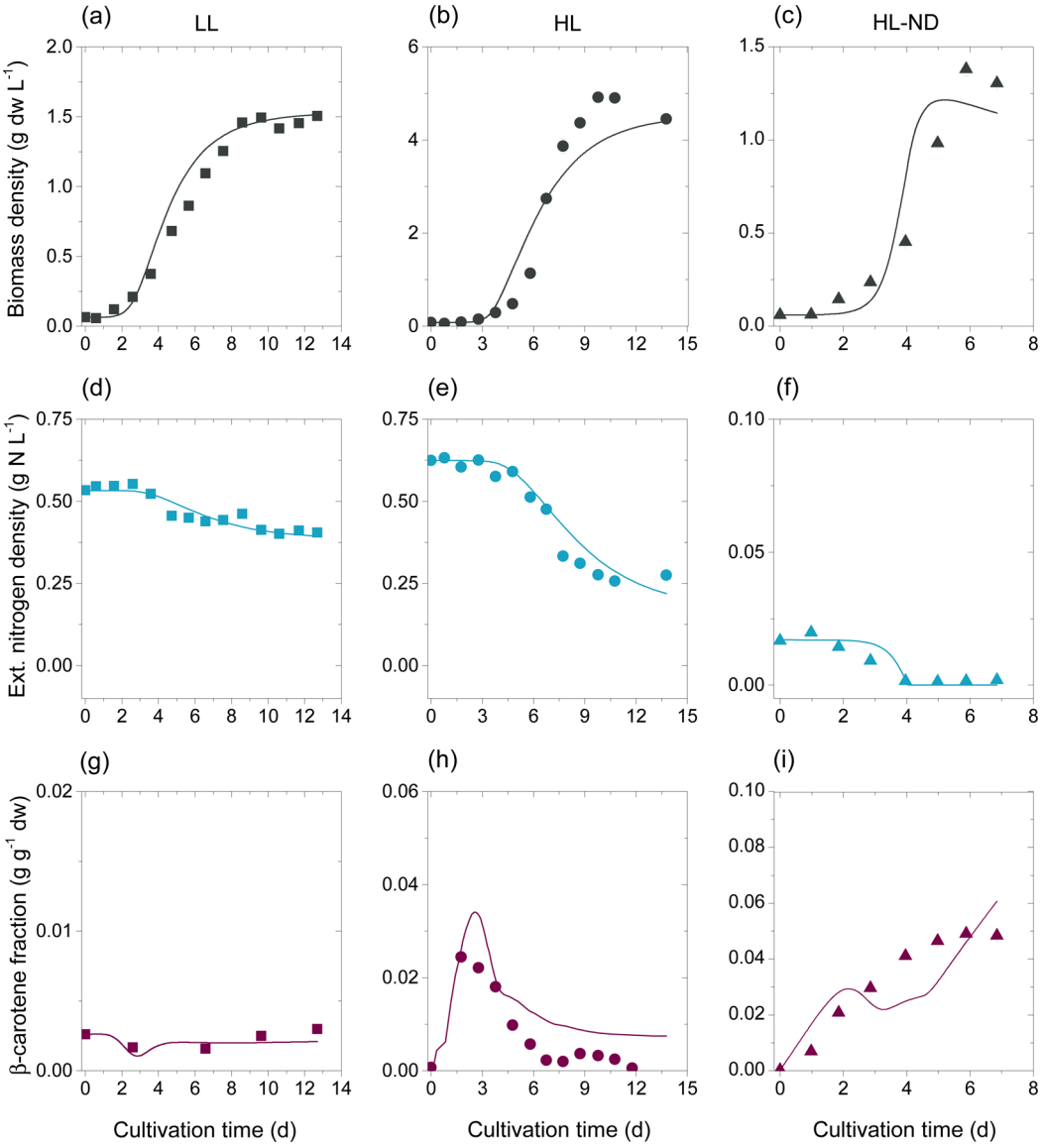

Figure 5. Model simulations for *D. parva* for the effect of various cultivation conditions on the biomass density ρ_X (a–c), the extracellular nitrogen density $\rho_{N,ext}$ (d–f), and the β-carotene fraction ω_{Car} (g–i). Comparison of the simulated time course (lines) with experimental data (symbols). The symbols represent the mean values and the error bars correspond to the standard deviation. An initial biomass density of 0.1 g dw L^{-1} was used for inoculation. The illumination of the reactor was performed as stated in Table S4 in the Supporting Information.

$$r_{Car} = r_{Car,E}\frac{E_{X,dw}^{k}}{E_{car,crit}^{k} + E_{X,dw}^{k}} + r_{Car,N}\left(1 - \frac{\omega_N^k}{\omega_{N,crit}^k + \omega_N^k}\right) \quad (2)$$

where $r_{Car,E}$ and $r_{Car,N}$ represent the maximal synthesis rate under light and nutrient stress. The half saturation coefficients for light and nutrient stress are denoted as $E_{car,crit}$ and $\omega_{N,crit}$. The Hill coefficient is represented by k and $E_{X,dw}$ is the light intensity per biomass. Please note that the cultivations for *D. parva* were conducted under constant light conditions and the average photon flux density $\overline{E}$ can be used instead of $E_{X,dw}$.

Growth rate. Since pronounced photoinhibitory effects were observed for growth of *D. salina* under high light conditions, a growth rate approach containing an inhibition term has been formulated to describe the specific biomass growth rate μ.[9] In addition, a Droop term has been added to the equation to ensure growth arrest under nitrogen depletion as shown in eq 3:[10]

$$\mu = \mu_{max}\frac{E_{X,dw}}{E_{X,dw} + K_{s,E}\frac{\rho_X}{\rho_{Chl}} + \frac{E_{X,dw}^2}{K_{i,E}}}\left(1 - \frac{\omega_{N,min}}{\omega_N}\right) \quad (3)$$

The following five dynamic equations are deduced from the algebraic equations in order to describe biomass growth, chlorophyll, and β-carotene fraction, extracellular nitrogen density and nitrogen quota:

$$\frac{d\rho_X}{dt} = \mu_{net}\rho_X \quad (4)$$

$$\frac{d\rho_{N,ext}}{dt} = -r_N\rho_X \quad (5)$$

$$\frac{d\omega_N}{dt} = r_N - \mu\omega_N \quad (6)$$

DOI: 10.1021/acs.iecr.7b01423
Ind. Eng. Chem. Res. XXXX, XXX, XXX–XXX

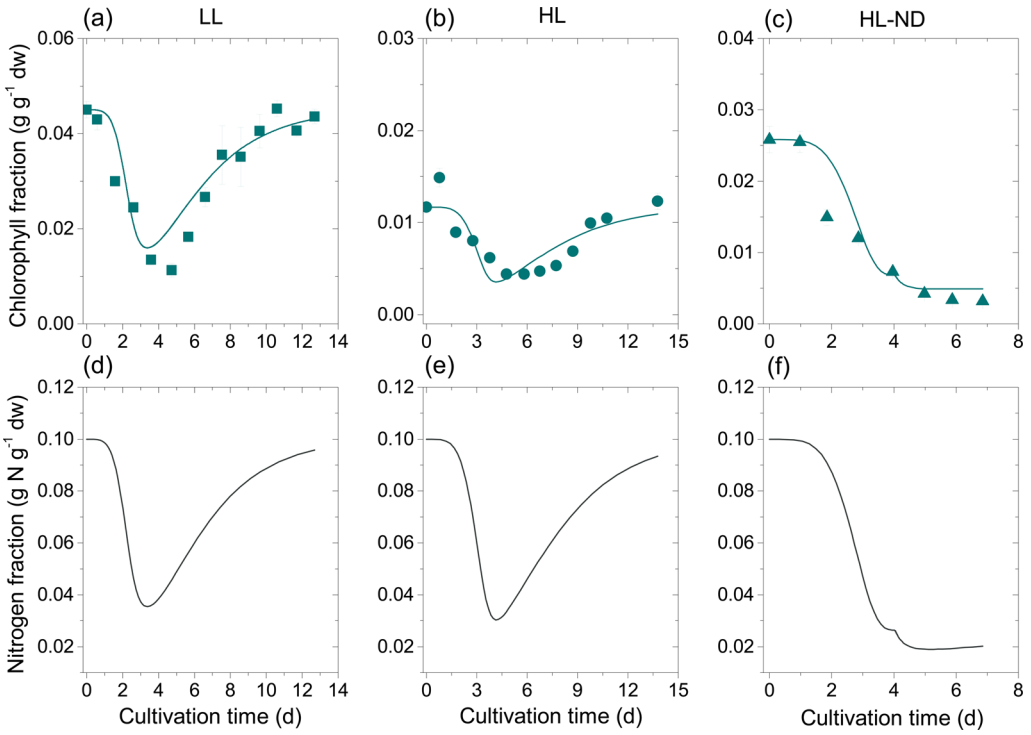

Figure 6. Model simulations for *D. parva* for the effect of various cultivation conditions on the chlorophyll fraction ω_{Chl} (a–c) and the nitrogen quota in the biomass ω_N (d–f). Comparison of the simulated time course (lines) with experimental data (symbols). The symbols represent the mean values and the error bars correspond to the standard deviation.

$$\frac{d\omega_{Chl}}{dt} = \frac{\omega_{Chl,N}\cdot\mu\cdot r_N}{r_P\cdot\left(\frac{\omega_{Chl}}{\omega_C}\right)} - \mu_{net}\omega_{Chl} \quad (7)$$

$$\frac{d\omega_{Car}}{dt} = r_{Car} - \mu_{net}\omega_{Car} \quad (8)$$

The model equations contain 9 parameters (optimization variables) and 11 biomass and three reactor constants (see Tables S6 and S7).

The proposed model was implemented in MATLAB (MathWorks) and solved by using CVODES.[11] The model simulations were compared with the experimental data of *D. salina* and *D. parva* grown under different cultivations conditions (Tables S2 and S3) in flat-plate photobioreactors in batch mode. The parameter estimation was performed using the nonlinear optimization algorithm fmincon with an initial parameter set based on literature and experimental data. This algorithm minimizes the objective function as defined in eq 9:

$$\chi^2(\Theta) = \sum_{k=1}^{m}\sum_{i=1}^{d_k}\frac{1}{\sigma_{ki}^2}(y_k(t_i) - y_k(t_i,\Theta))^2 \quad (9)$$

where m is the number of measured outputs, d_k is the number of measurement times, y_k and $\hat{y}_k$ are the kth measured output variable and corresponding model prediction and σ_{ki}^2 is the variance in the measured data.

Parameter Estimation. The nine model parameters of the proposed equation system were estimated to describe the dynamic changes in the biomass density, the chlorophyll, and β-carotene fraction as well as the extracellular nitrogen density in largest agreement to the experimental data. For this purpose, the objective function was defined to minimize the weighted sum of squared residuals (eq 9) for ρ_X, ω_{Chl}, ω_{Car}, and $\rho_{N,ext}$ for three experimental conditions (see LL, HL, and HL-ND in Tables S2 and S3). According to the measurement, results for the biomass-specific parameters of *D. salina* and *D. parva* were set as shown in Tables S6 and S7. Box constraints were imposed on the parameters according to biophysical limitations. The measurement variances were parametrized as $\sigma_{ki}^2 = 0.1\ \max(y_k(t))$.

Profile Likelihood Analysis of Model Parameters. The reliability and identifiability of the estimated parameter set was studied using profile likelihood analysis. The approach was proposed by Raue et al.[12] and is based on constrained likelihood profiles. The systematic exploration of the high-dimensional parameter space is done individually for each parameter (Θ_i) with respect to all other parameters $\Theta_{j\neq i}$ as shown in eq 10.[13]

$$\chi_{PL}^2(\Theta_i) = \min_{\Theta_{j\neq i}}[\chi^2(\Theta)] \quad (10)$$

On the basis of the shape of $\chi_{PL}^2(\Theta_i)$, one can distinguish between structural and practical identifiability or nonidentifiability. Structural and practical identifiable parameters have a parabolically shaped $\chi_{PL}^2(\Theta_i)$ curve and nonidentifiable parameters have a χ_{PL}^2 curve with a flat shape. If the flat shape occurs in the direction of one confidence bound, the parameters are practical nonidentifiable, whereas in the direction of both confidence bounds structural nonidentifiability occurs. The profile likelihood algorithm was implemented in MATLAB. Absolute and relative tolerances have been set to 10^{-7} and 10^{-6}, respectively.

Results for *D. salina*. *Biomass Growth under Fluctuating Light and Nutrient Conditions.* The simulation results shown in Figure 2a–c demonstrate that the model describes the dynamics of biomass growth under various light and nutritional conditions with the estimated parameter set $\hat{\Theta}$ (Table 1) in a

DOI: 10.1021/acs.iecr.7b01423
Ind. Eng. Chem. Res. XXXX, XXX, XXX–XXX

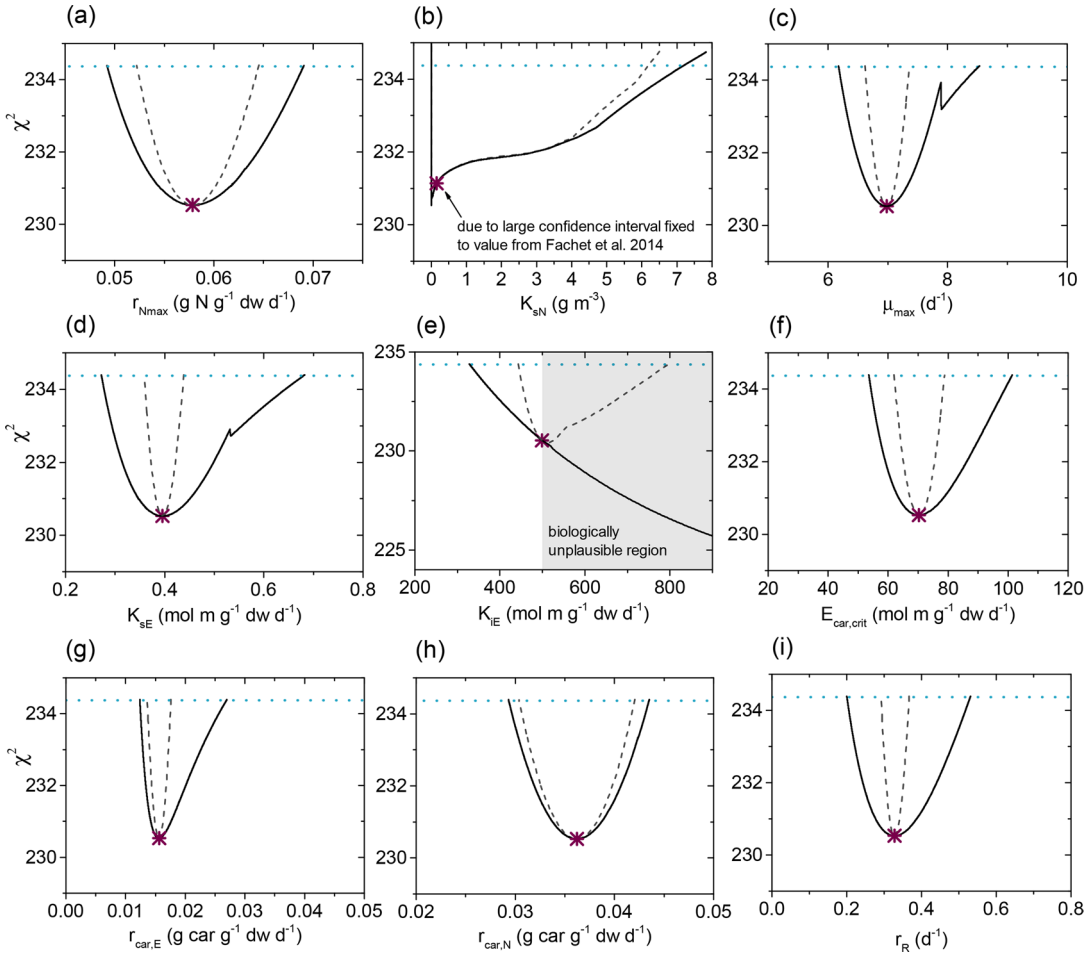

Figure 7. Profile likelihood-based identifiability for all model parameters for *D. parva*: (a) maximal nitrogen uptake rate r_{max}, (b) half-saturation coefficient for nitrogen uptake $K_{s,N}$, (c) maximal growth rate μ_{max}, (d) half-saturation coefficient for photosynthetic growth $K_{s,E}$, (e) light inhibition coefficient for photosynthetic growth $K_{i,E}$, (f) critical light intensity for β-carotene synthesis $E_{car,crit}$, (g) light stress-induced β-carotene synthesis rate $r_{car,E}$, (h) nutrient stress-induced β-carotene synthesis rate $r_{car,N}$ and (i) respiration rate, r_R. The profile likelihood-based sensitivity curve, where Θ_i is varied and all other parameters $\Theta_{j\neq i}$ are kept constant, is indicated by the dashed gray line. The profile likelihood-based identifiability curves are indicated by the black solid line. The blue dotted horizontal line indicates the threshold utilized to assess likelihood-based 95% confidence interval and the asterisk corresponds to the optimal parameter value.

Table 2. Optimal Parameter Values $\hat{\Theta}$ as Well as the Individual Confidence Intervals $[\sigma_i^-; \sigma_i^+]$ Corresponding to a Confidence Level of 95% from Constrained Nonlinear Optimization and Profile Likelihood Analysis for *D. parva* in Comparison with *D. salina*

strain	symbol	$\hat{\Theta}$ for *D. salina*	$\hat{\Theta}$ for *D. parva*	σ_i^-	σ_i^+	identifiability
D. parva	$r_{N,max}$	0.346	0.058	0.049	0.069	structurally and practically identifiable
	$K_{s,N}$	0.05	0.155	0	7.832	structurally and practically identifiable
	μ_{max}	1.708	6.980	6.176	8.533	structurally and practically identifiable
	$K_{s,E}$	0.033	0.396	0.272	0.682	structurally and practically identifiable
	$K_{i,E}$	68.7190	499	328.078	$+\infty$	practical nonidentifiable, biologically plausible
	$E_{car,crit}$	77.718	70.202	53.564	101.429	structurally and practically identifiable
	$r_{car,E}$	0.032	0.016	0.012	0.026	structurally and practically identifiable
	$r_{car,N}$	0.005	0.036	0.029	0.043	structurally and practically identifiable
	r_R	0.142	0.327	0.200	0.531	structurally and practically identifiable

good manner. The maximum biomass density from all three experimental conditions was achieved in the cultivation under low light (LL), namely 7.2 g dw L^{-1}. This corresponds to a final cell density of 1.4×10^7 cells mL^{-1} cultivation volume. The final biomass density reached in the stationary phase for the cultivations under high light (HL) is 6.5 g dw L^{-1} and almost comparable to the low light condition (LL). Under high light and nitrogen depletion (HL-ND) the biomass growth was significantly lowered due to nutrient abundance and only 1.1 g dw L^{-1} biomass was achieved.

Extracellular Nitrogen Uptake. The simulated time course for the extracellular nitrogen density agreed well with the experimental data (Figure 2d–f). The results revealed that the growth under all three conditions was always nutrient and never light-limited. As expected, the growth under nutrient-depleted conditions (HL-ND) was governed by the lowest

DOI: 10.1021/acs.iecr.7b01423
Ind. Eng. Chem. Res. XXXX, XXX, XXX−XXX

external nutrient availability and the internal nutrient status of the cells. The external nitrogen was totally depleted 4 days after inoculation in the nitrogen starved culture (HL-ND). The simulation results clearly indicate that nitrogen uptake is strongly reduced in the *lag* phase under nitrogen-repleted conditions (LL, HL), since the nitrogen cell quota is close to its maximal value $\omega_{N,max}$ (Figure 2d−f).

The predicted maximal nitrogen uptake rate is 0.346 g N g^{-1} dw d^{-1}. The value for the calculated nitrogen uptake rate $r_{N,}$ under all three conditions is approximately 0.05 g N g^{-1} dw d^{-1}, which is in good agreement with measurements ranging from 0.05−0.015 g N g^{-1} dw d^{-1} measured for several green microalgal species by Hein et al.[14] However, it is lower than measured nitrogen uptake rates for the same strain used in this study, namely *D. salina* CCAP 19/18, grown in a low light turbidostat culture (0.085 g N g^{-1} dw d^{-1}) measured by Lamers et al.[15] and 0.08 g N g^{-1} dw d^{-1} from Lomas and Glibert[16] measured for the closely related organism *D. tertiolecta*.

β-Carotene Fraction in the Biomass. The model simulations agree well with the experimental data for the β-carotene fraction ω_{Car} in the cells (Figure 2g−i). The data clearly indicate that light and nutrient stress alone are able to induce the accumulation of the photoprotective pigments. However, when both stress conditions are combined under HL-ND conditions the β-carotene synthesis exceeds the fractions achieved under LL or HL conditions. The highest β-carotene fraction was detected in the HL-ND culture with 8.0% (w/w), followed by the HL culture with 4.3% (w/w) at day 3 and 2.7% (w/w) in the stationary culture under LL conditions. Under HL conditions the initially high β-carotene accumulation induced by the presence of light stress declined as soon as the incident light intensity fell below the fixed light stress of 3000 μmol m^{-2} s^{-1} g^{-1} dw L due to the physical limitation of the LED light panel to a maximal light intensity of 3000 μmol m^{-2} s^{-1}. Under LL conditions, the β-carotene synthesis started when a critical nitrogen quota of approximately 0.075 g N g^{-1} dw was reached.

Total Chlorophyll Fraction in the Biomass. The model simulations agree reasonably well with the experimental data for the chlorophyll fraction ω_{Chl}, which is crucial for predicting the light attenuation in the reactor (Figure 3a−c). During the initial cultivation period more light energy is supplied per cell than is required for growth, resulting in a considerable decline of the total chlorophyll fraction under all three conditions. The minimal total chlorophyll content in the biomass is almost comparable under three cultivation conditions, namely 0.004 g Chl g^{-1} dw.

Identifiability Analysis Using the Profile Likelihood. The results of the identifiability analysis of all model parameters using likelihood profiles are presented in Figure 4. This approach allows distinguishing between structural nonidentifiable, practical nonidentifiable, and identifiable parameters depending on the shape of χ^2_{PL} as discussed in Fachet et al.[8] The lower and upper bounds of the 95% confidence intervals are given in Table 1. All nine model parameters are identifiable indicated by the shape of the χ^2_{PL} curve and the finite size of the derived confidence intervals (Figure 4a−i, black solid line, and Table 1). Besides profile likelihood, likelihood analysis is frequently performed to evaluate the predictive power of a proposed model. In contrast to the profile likelihood, where one parameter Θ_i is varied and all other parameters $\Theta_{j\neq i}$ are reoptimized, for conventional likelihood analysis only the parameter value for Θ_i is changed and the remaining parameters $\Theta_{j\neq i}$ are kept constant. Because of this, the parameter identifiability analysis using the likelihood function is less strict than the profile likelihood-based identifiability analysis. This is illustrated in Figure 4 (gray dashed lines vs black solid lines). Still, likelihood analysis is useful to identify potentially nonidentifiable parameters.

The likelihood of the nine identifiable model parameters seems to be in an asymptotic setting indicated by the parabolic shape with finite size of the 95% confidence interval (Figure 4a−i). Because of the negligence of the parameter interdependencies, the confidence interval derived for each parameter are significantly smaller for the likelihood-based derivation compared to the profile likelihood. This example illustrates the strength of the identifiability analysis based on profile likelihoods leading to detailed information about parameter interdependencies and reliable confidence intervals. The application of optimal experimental design (OED) approaches could be beneficial in order to determine the measurement signal with the highest information content.[17,18]

Results for *D. parva*. *Biomass Growth under Fluctuating Light and Nutrient Conditions.* Similar to the results for *D. salina*, the simulation results for *D. parva* are in good agreement with the experimental data (Figures 5 and 6). The observed growth behavior under HL conditions confirmed the result of the PAM analysis that *D. parva* showed no pronounced photoinhibitory effects (Figure 1b). The highest biomass density on dry weight basis was reached under HL conditions, namely 4.9 g dw L^{-1}. The final biomass densities in the stationary phases of the LL and HL-ND conditions are almost the same, namely 1.5 g dw L^{-1} and 1.4 g dw L^{-1}.

Extracellular Nitrogen Uptake. The dynamics in the extracellular nitrogen uptake agree well with the experimental data (Figure 5). The results indicate that the growth under LL and HL conditions (nutrient repletion) was always limited by the availability of light. The growth under nutrient-depleted conditions (HL-ND) was governed by the extracellular nitrogen density, where a complete depletion occurred 4 days after inoculation. The dynamics of the intracellular nitrogen quota ω_N clearly show that nitrogen uptake is down-regulated in the early exponential and late stationary growth phase under nitrogen repletion (LL and HL conditions), since ω_N is close to the maximal quota $\omega_{N,max}$.

β-Carotene Fraction in the Biomass. The light and nutrient dependency on the β-carotene synthesis works in the same way for *D. parva* as observed for *D. salina* (eq 2). The highest β-carotene fraction was achieved during a combination of light stress and nutrient stress. However, the maximal mass fraction for *D. parva* is 4.9% (w/w) significantly lower compared to that of *D. salina* being 8.0% (w/w).

Total Chlorophyll Fraction in the Biomass. For the total chlorophyll content in the biomass ω_{Chl}, a good agreement between simulation results and experimental data is observed (Figure 6). Exactly as detected for *D. salina*, *D. parva* shows a considerable degradation of chlorophyll in the initial cultivation period. This is caused by an imbalance in photon supply compared to the photons required for growth. The extent of the chlorophyll degradation strongly depends on the average light intensity in the reactor. For cells cultivated under nitrogen repletion (LL and HL conditions), an accumulation of chlorophyll is observed in the exponential phase to increase the light harvesting efficiency under light limiting conditions. This behavior of chlorophyll synthesis under light limiting conditions has only been observed for *D. parva* and not for *D. salina* (see Figure 3). Since growth and chlorophyll synthesis

DOI: 10.1021/acs.iecr.7b01423
Ind. Eng. Chem. Res. XXXX, XXX, XXX−XXX

are strongly impaired during nitrogen starvation, the chlorophyll content in the biomass steadily decreases from 42 mg g^{-1} dw to 5 mg g^{-1} dw.

The optimal parameter estimates and the identifiability of the nine model parameters for *D. parva* are given in Figure 7 and Table 2. Whereas in the *D. salina* growth model all parameters were identifiable, in the *D. parva* growth model one parameter was practically nonidentifiable, namely the light inhibition coefficient for photosynthetic growth $K_{i,E}$. Since *D. parva* showed no pronounced photoinhibitory effects it is biologically plausible that the corresponding parameter $K_{i,E}$ is not identifiable indicated by the flat profile likelihood in direction of the upper confidence bound. The halfsaturation coefficient for nitrogen uptake $K_{S,N}$ was fixed to a value of 0.155 g m^{-3}, which was recalculated from experimental data for *Dunaliella tertiolecta* from Lomas and Glibert[16] and has already been used for the growth model published by Fachet et al.[8] The confidence intervals calculated for the parameters $K_{S,N}$ and $K_{i,E}$ are higher for *D. parva* compared to *D. salina*. This illustrates the strength of the profile likelihood analysis in comparison to the frequently used likelihood analysis in which one parameter is varied and the remaining parameters are kept constant. Large confidence intervals in the profile likelihood result from structural dependencies between different model parameters. For this reason, the profile likelihood derived confidence intervals are much more informative with regard to (i) identifiability, (ii) detection of (nonlinear) parameter interdependencies, and (iii) consistency in confidence interval estimates compared to likelihood derived (individual) confidence intervals. This also holds for classical Hessian-based estimates of confidence intervals, which only yield consistent approximations for identifiable parameters.

In agreement with the PAM measurements (Figures 1a,b) for which *D. parva* showed a significantly higher ETR compared to *D. salina*, the better photosynthetic growth potential is also reflected by the parameter estimates for the maximal growth rate (μ_{max}) and the half saturation coefficient for photosynthetic growth ($K_{s,E}$) as shown in Table 2. The optimal parameter estimates obtained for *D. parva* are notably higher compared to *D. salina*, namely 6.980 to 1.708 d^{-1} for μ_{max} and 0.396 to 0.033 mol photons m g^{-1} dw d^{-1} for $K_{s,E}$. Because of the small cell weight of *D. parva* (Table S1), the higher photosynthetic growth potential does not translate into a more productive cultivation process since the biomass productivity of *D. parva* is considerably lower compared to that of *D. salina* (see Table S5). However, the strain selection of *D. parva* for an outdoor cultivation process might be beneficial because of its absence of photoinhibition under high irradiance.

In this work, the β-carotene content under HL-ND conditions for *D. salina* was 80 mg g^{-1} dw, 63% higher than the 49 mg g^{-1} dw measured for *D. parva*. Therefore, also the parameter for the light stress-induced β-carotene synthesis rate $r_{car,E}$ is 2-fold higher for *D. salina* (0.032 g Car g^{-1} dw d^{-1} to 0.016 g Car g^{-1} dw d^{-1} for *D. parva*). However, the critical light intensity for β-carotene synthesis ($E_{car,crit}$) is almost comparable (70 mol photons g^{-1} dw d^{-1} for *D. parva* and 78 mol photons g^{-1} dw d^{-1} for *D. salina*).

CONCLUSIONS

In this work, a systematic approach for analysis of interspecies variability with the case study of β-carotene production in the *Dunaliella* species *D. salina* and *D. parva* in a photobioreactor setup was presented. The results of the experimental comparison indicated significant variability between *D. salina* and *D. parva* in terms of morphological differences, the biomass, and β-carotene productivity as well as differences in photoacclimation and photoinhibition. The experimental data was used to formulate a dynamic-kinetic model. The ordinary differential equation system accounted for biomass growth, nutrient uptake, and pigment fraction in the biomass and was able to describe the both species in a good manner. The proposed model structure was a trade-off between the justification of the experimentally observed behavior under various abiotic stress conditions with a minimal number of parameters. In agreement with the experimental results, the optimal parameter values estimated for *D. salina* and *D. parva* showed significant interspecies deviations. The profile likelihood analysis demonstrated that the majority of the model parameters were structurally and practically identifiable giving evidence of its predictivity. The ongoing methodological advances in the experimental as well as the computational area will further broaden our knowledge on the metabolic adaption of microalgae and lead to a progressive improvement of mathematical models. Thereby, the engineering of industrially valuable strains is accelerated and provides the basis for effective bioprocess design with photosynthetic microorganisms.

ASSOCIATED CONTENT

Supporting Information

The Supporting Information is available free of charge on the ACS Publications website at DOI: 10.1021/acs.iecr.7b01423.

Overview of experimental conditions; biotechnological performance of *D. salina* and *D. parva*; model equations; overview of parameters from dynamic-kinetic model (PDF)

AUTHOR INFORMATION

Corresponding Author

*E-mail: rihko@mpi-magdeburg.mpg.de.

ORCID

Liisa K. Rihko-Struckmann: 0000-0003-0222-7236

Notes

The authors declare no competing financial interest.

ACKNOWLEDGMENTS

This research work was partly supported by the Center for Dynamic Systems (CDS) in Magdeburg/Germany, funded by the EFRE funds of the German Federal State Saxony-Anhalt. The authors gratefully thank Anne Christin Reichelt and Markus Ikert for their technical support in pigment extraction and detection as well as Isabel Harriehausen for supporting the cultivations, the flow cytometric analysis, and the PAM measurements.

REFERENCES

(1) Polle, J. E. W.; Tran, D.; Ben-Amotz, A. In *The Alga Dunaliella: Biodiversity, Physiologoy, Genomics and Biotechnology*, 1st ed.; Ben-Amotz, A., Polle, J. E. W., Rao, D. V. S., Ed.; Science Publishers: Enfield, 2009; Chapter 1, pp. 1−13.

(2) Ben-Amotz, A.; Shaish, A.; Avron, M. The biotechnology of cultivating Dunaliella for production of β-carotene rich algae. *Bioresour. Technol.* **1991**, *38*, 233−235.

(3) Gonzalalez, M. A.; Gomez, P. I.; E. W. Polle, J. In *The Alga Dunaliella: Biodiversity, Physiologoy, Genomics and Biotechnology*, 1st ed.;

DOI: 10.1021/acs.iecr.7b01423
Ind. Eng. Chem. Res. XXXX, XXX, XXX−XXX

Ben-Amotz, A., Polle, J. E. W., Rao, D. V. S., Ed.; Science Publishers; Enfield, 2009; Chapter 2, pp. 15−43.
(4) Lichtenthaler, H. K. *Current Protocols in Food Analytical Chemistry*; Wiley, 2001.
(5) Fachet, M.; Hermsdorf, D.; Rihko-Struckmann, L.; Sundmacher, K. Flow cytometry enables dynamic tracking of algal stress response: A case study using carotenogenesis in Dunaliella salina. *Algal Res.* **2016**, *13*, 227−234.
(6) Borowitzka, M. A.; Siva, C. J. The taxonomy of the genus Dunaliella (Chlorophyta, Dunaliellales) with emphasis on the marine and halophilic species. *J. Appl. Phycol.* **2007**, *19*, 567−590.
(7) Schreiber, U.; Klughammer, C.; Kolbowski, J. *PAM Application Notes* **2011**, *1*, 1−21.
(8) Fachet, M.; Flassig, R. J.; Rihko-Struckmann, L.; Sundmacher, K. A dynamic growth model of Dunaliella salina: Parameter identification and profile likelihood analysis. *Bioresour. Technol.* **2014**, *173C*, 21−31.
(9) Mairet, F.; Bernard, O.; Lacour, T.; Sciandra, A. Modelling microalgae growth in nitrogen limited photobiorector for estimating biomass, carbohydrate and neutral lipid productivities. *Preprints of the 18th IFAC World Congress* **2011**, *44*, 10591−96.
(10) Droop, M. R. Vitamin B12 and Marine Ecology. IV. The Kinetics of Uptake, Growth and Inhibition in Monochrysis Lutheri. *J. Mar. Biol. Assoc. U. K.* **1968**, *48*, 689−733.
(11) Hindmarsh, A. C.; Brown, P. N.; Grant, K. E.; Lee, S. L.; Serban, R.; Shumaker, D. E.; Woodward, C. S. *Acm Transactions on Mathematical Software* **2005**, *31*, 363−396.
(12) Raue, A.; Kreutz, C.; Maiwald, T.; Bachmann, J.; Schilling, M.; Klingmüller, U.; Timmer, J. Structural and practical identifiability analysis of partially observed dynamical models by exploiting the profile likelihood. *Bioinformatics* **2009**, *25*, 1923−1929.
(13) Kreutz, C.; Raue, A.; Kaschek, D.; Timmer, J. Profile likelihood in systems biology. *FEBS J.* **2013**, *280*, 2564−2571.
(14) Hein, M.; Pedersen, M. F.; Sand-Jensen, K. Size-dependent nitrogen uptake in micro- and macroalgae. *Mar. Ecol.: Prog. Ser.* **1995**, *118*, 247−253.
(15) Lamers, P. P.; Janssen, M.; De Vos, R. C. H.; Bino, R. J.; Wijffels, R. H. Carotenoid and fatty acid metabolism in nitrogen-starved Dunaliella salina, a unicellular green microalga. *J. Biotechnol.* **2012**, *162*, 21−27.
(16) Lomas, M. W.; Glibert, P. M. Comparisons of Nitrate Uptake, Storage, And Reduction in Marine Diatoms and Flagellates. *J. Phycol.* **2000**, *36*, 903−913.
(17) Muñoz-Tamayo, R.; Martinon, P.; Bougaran, G.; Mairet, F.; Bernard, O. Getting the most out of it: Optimal experiments for parameter estimation of microalgae growth models. *J. Process Control* **2014**, *24*, 991−1001.
(18) Flassig, R. J.; Migal, I.; der Zalm, E. v.; Rihko-Struckmann, L.; Sundmacher, K. Rational selection of experimental readout and intervention sites for reducing uncertainties in computational model predictions. *BMC Bioinf.* **2015**, *16*, 13.

DOI: 10.1021/acs.iecr.7b01423
Ind. Eng. Chem. Res. XXXX, XXX, XXX−XXX